Journal of
Applied Crystallography
ISSN 0021-8898

Received 10 June 2005
Accepted 11 October 2005

Structure of the quaternary alloy $Zn_{0.6}Mn_{0.4}In_2S_4$ from synchrotron powder diffraction and electron transmission microscopy

Rosario Ávila-Godoy,[a] Asiloé J. Mora,[b]* Dwight R. Acosta-Najarro,[c] Gerzon E. Delgado,[b] Santos A. López-Rivera,[a] Andrew N. Fitch,[d] Andrés E. Mora[a,e] and John W. Steeds[e]

[a]Departamento de Física, Universidad de Los Andes, Mérida, Venezuela, [b]Departamento de Química, Universidad de Los Andes, Mérida, Venezuela, [c]Instituto de Física, Universidad Nacional Autónoma de México, México DF, México, [d]European Synchrotron Radiation Facility, Grenoble CEDEX, France, and [e]Physics Department, University of Bristol, Bristol BS8 1TL, UK. Correspondence e-mail: asiloe@ula.ve

The aim of the present work was to determine the structure of the quaternary alloy $Zn_{0.6}Mn_{0.4}In_2S_4$ and to locate the Mn^{2+}. This was accomplished by means of powder synchrotron X-ray diffraction, high-resolution microscopy and convergent-beam electron diffraction (CBED). The powder X-ray diffraction pattern was indexed in a rhombohedral cell, with cell constants $a = 3.875$ (2), $c = 37.208$ (4) Å, and possible space groups $R\bar{3}m$ or $R3m$. Rietveld refinements using different cationic arrangements in these space groups were performed. A model in space group $R3m$, in which the tetrahedral and octahedral sites were occupied by different proportions of Zn, Mn and In atoms, gave the best result. The Rietveld refinement of this model led to figures of merit $R_{wp} = 9.8\%$, $R_p = 9.1\%$ and $\chi^2 = 11.1$. Selected-area electron diffraction patterns and high-resolution transmission electron micrographs along [001] reveal the rhombohedral configuration. CBED patterns perpendicular to [001], showing the distinctive $3m$ symmetry, confirmed space group $R3m$ and the breaking of the centrosymmetry of the parent compound, $ZnIn_2S_4$.

1. Introduction

The quaternary alloy $Zn_{0.6}Mn_{0.4}In_2S_4$ is a member of the family of defect semiconductors which originates from the ternary systems $ZnIn_2S_4$ and $MnIn_2S_4$. These end groups have different crystal structures that show some degree of disorder. There are three structural reports for $MnIn_2S_4$. Two of them show a partially inverse spinel structure belonging to the space group $Fd\bar{3}m$, with the lattice parameter a being close to 10.719 Å (Wakaki *et al.*, 1983; Lutz & Jun, 1989). In the third report, $MnIn_2S_4$ is a cubic $F\bar{4}3m$ structure with $a = 10.720$ Å (Lutz & Jun, 1989). The other member, $ZnIn_2S_4$, shows a wurtzite-like structure and is considered to be the prototype of layered semiconductors. It has been thoroughly investigated owing to the outstanding anisotropy in its properties, the presence of polytypes and the possibility of intercalating diverse types of species between its layers (Atwood *et al.*, 1984). The range of inter-solubility is not well known; however, the phase diagram of the binary system ZnS–MnS, reported by Sombuthawee *et al.* (1978), has been used to establish that the ternary system $ZnIn_2S_4$–$MnIn_2S_4$ should show similar structural characteristics. Therefore, the transition from wurtzite to zinc blende observed in the binary system at 40–50% of MnZn should also be observed in the ternary system for a similar composition. The optical absorption and photoluminescence spectra, interpreted using crystal field analysis (Pineda *et al.*, 1998), show that the Mn atoms occupy tetrahedral positions in $R\bar{3}m$ symmetry. On the other hand, the magnetic properties, reported by Sagredo *et al.* (1993), show that the Mn^{2+} ions could be placed at random in tetrahedral and octahedral sites in a non-centrosymmetric $R3m$ structure. The analysis of the mid-IR spectra (Fontal *et al.*, 1996), in the 800–400 cm^{-1} region, suggest that the Mn^{2+} ions replace the Zn^{2+} ions in the tetrahedral sites, close to the S...S interlayer of the $R\bar{3}m$ structure of the parent compound, $ZnIn_2S_4$ (Berand & Range, 1994). Tatsi *et al.* (2002) studied the compositions $Zn_{0.6}Mn_{0.4}In_2S_4$ and $Zn_{0.7}Mn_{0.3}In_2S_4$ under hydrostatic pressures and ambient conditions, and suggest that the crystal structures of these compounds are $R\bar{3}m$. It is evident that contradictory results point towards two different crystal structures: centrosymmetric $R\bar{3}m$ and non-centrosymmetric $R3m$. The difference between the structures is based only on the cation distribution and its degree of disorder in the different crystal sites. The elucidation of the structure to this degree of precision requires the best diffraction data from a highly crystalline material. However, this could be difficult to achieve considering that it is known that $ZnIn_2S_4$ exists as different polytypes depending

on the method of growth, which generate a large number of crystalline defects that limit the precise knowledge of the distribution of the atoms in the unit cell. On the other hand, when the solid solution $Zn_{0.6}Mn_{0.4}In_2S_4$ forms, the material departs from the stoichiometry of the parent compound $ZnIn_2S_4$; therefore, it is likely that some cation sites lose the $3m$ point symmetry owing to the need to place different proportions of Zn, In and Mn in these sites. This might induce a change in the crystal symmetry from $R\bar{3}m$ to $R3m$. Finally, it is necessary to inquire about the likelihood of placing the magnetic ions Mn^{2+} in tetrahedral sites or octahedral sites in the unit cell of $Zn_{0.6}Mn_{0.4}In_2S_4$.

2. Experimental

2.1. Synthesis

Stoichiometric amounts of ZnS, MnS and In_2S_3 were pulverized to small grain size, mixed and compacted into cylindrical pellets at a pressure of 1300 MPa. These pellets were then placed into quartz capsules under vacuum and heated to 1373 K for 48 h. Yellow sheet-like crystals were grown by the chemical-transport technique using iodine as transporting agent, and heating the sample at 1773 K, above the melting point of $ZnIn_2S_4$ (Giriat, 1985). The chemical composition of the alloy, confirmed from energy dispersive X-ray spectra (EDX) at 20.48 kV in a Jeol 5600 Electron Microscope, gave the atomic ratios Zn:Mn:In:S 0.59:0.39:2.0:4.0, which matched the nominal composition within 0.01. The error in standardless analysis was around 5%.

2.2. X-ray diffraction

For the X-ray analysis, a small quantity of the alloy was ground in an agate mortar and pestle, avoiding any excess of pressure, to prevent the degradation of the crystalline quality of the material. The resulting powder was mounted on a flat zero-background silicon [511] crystal holder, covered with a thin layer of petroleum jelly. Diffraction data were collected on a Siemens D5005 diffractometer, set up in θ/θ reflection mode, equipped with a diffracted-beam graphite monochromator and an X-ray tube (Cu $K\alpha$ radiation: $\lambda = 1.54059$ Å, 30 kV, 15 mA). A fixed aperture and divergence slit of 1 mm, a 0.1 mm monochromator slit, and a 0.6 mm detector slit were used. Patterns were recorded between 5 and 100° 2θ, with increments of 0.02°, counting at each step for 35 s.

For the Rietveld analysis, improved diffraction data were collected on the high-resolution powder diffractometer of beamline ID31 at the European Synchrotron Radiation Facility (ESRF), in Grenoble, France, using a wavelength of 0.499229 (5) Å taken from an undulator source (Fitch, 1996, 2004). For these experiments, specimens were prepared in borosilicate capillaries, 0.5 mm in diameter, sealed at one end and spun at 100 r.p.m on the axis of the diffractometer to improve randomization of the individual crystallite orientations.

2.3. Electron microscopy

The morphological study and chemical composition analysis of the samples were carried out in a Jeol-5600 Scanning Electron Microscope (SEM) equipped with a Noran X-ray detector. The electron diffraction patterns were obtained in a Jeol CX-100 electron microscope, while the high-resolution electron images and the convergent-beam diffraction patterns were recorded in a Jeol-EX4000 and in a Philips EM-430 electron microscope, respectively. In the latter a double-tilt holder was required. All the micrographs were digitized in a CCD camera. For the different transmission microscopy studies, crystals with exactly defined thickness were used. The crystallographic study was carried out using the *CRISP* program (Hovmöller, 1992).

3. Results

3.1. X-ray structure analysis

Preliminary experiments using a laboratory diffractometer using Bragg–Brentano reflection symmetry clearly showed that this material is greatly affected by preferred orientation, particularly with reflection 009. Therefore, it was necessary to perform diffraction experiments on the parallel-beam diffractometer of beamline ID31 at the ESRF, which allows the collection of diffraction data in capillary-transmission mode.

The pattern was indexed using the auto-indexing program *DICVOL91* (Boultif & Louër, 1991) with figures of merit $M_{(20)} = 44.0$ (de Wolff, 1968) and $F_{(30)} = 37.7$ (Smith & Snyder, 1979). Cell parameters are $a = 3.875$ (2) and $c = 37.208$ (4) Å.

Evaluation of the systematic absences shows that the condition of reflection is $-h + k + l = 00l = 3n$. This condition establishes that the possible space groups are $R3m$ (No. 160) and $R\bar{3}m$ (No. 166). As starting models, those of Berand & Range (1994), for space group $R\bar{3}m$, and Lappe *et al.* (1962), for $R3m$, were used.

Different cationic arrangements were assessed using the Rietveld (1967) method. The models were introduced into the program *GSAS* (Larson & von Dreele, 2001) using as starting cell parameters those obtained from the refinement of the laboratory diffraction data. The background was modelled using the automatic linear extrapolation of 15 points throughout the whole pattern. The peak shapes were modeled using a pseudo-Voigt peak shape function that included the axial divergence asymmetry correction (van Laar & Yelon, 1984; Finger *et al.*, 1994). Two isotropic temperature factors were refined, one for the Zn, Mn and In ions, and the other for the S atoms. Preferred orientation was corrected using the March–Dollase model (Dollase, 1986). However, this problem, particularly deleterious in these types of lamellar materials, is still present, as depicted in the exceptionally intense 009 reflection. Table 1 shows the results for the different structural models tested.

3.1.1. Centrosymmetric model in the $R\bar{3}m$ space group. Berand & Range (1994) and López-Rivera *et al.* (2001) described the structure of the ternary compound $ZnIn_2S_4$ in

Table 1
Allowed cationic distributions for the quaternary alloy $Zn_{0.6}Mn_{0.4}In_2S_4$.

Models constructed from Berand & Range (1994) ($R\bar{3}m$) and Lappe *et al.* (1962) ($R3m$). Occ. = occupancy; Tet = tetrahedral; Oct = octahedral.

Model	Atom	Site	x	y	z		Occ.	R_{wp} (%)	R_p (%)	χ^2
$R\bar{3}m$										
I	Zn	6*c*	0	0	0.77	Tet	0.3			
	Mn						0.2			
	In						0.5			
	In	3*a*	0	0	0	Oct	1.0	28.5	25.3	92.8
$R3m$										
I	Zn	3*a*	0	0	0.40	Tet	0.6			
	Mn						0.4			
	In	3*a*	0	0	0.17	Oct	1.0			
	In	3*a*	0	0	0.93	Tet	1.0	16.7	14.3	32.0
II	Zn	3*a*	0	0	0.40	Tet	0.6			
	In						0.4			
	Mn	3*a*	0	0	0.17	Oct	0.4			
	In						0.6			
	In	3*a*	0	0	0.93	Tet	1.0	11.3	10.1	14.5
III	Zn	3*a*	0	0	0.40	Tet	0.6			
	In						0.4			
	Mn	3*a*	0	0	0.17	Oct	0.2			
	In						0.8			
	Mn	3*a*	0	0	0.93	Tet	0.2			
	In						0.8	16.5	14.0	31.1
IV	Zn	3*a*	0	0	0.40	Tet	0.4			
	Mn						0.2			
	In						0.4			
	Zn	3*a*	0	0	0.17	Oct	0.2			
	Mn						0.2			
	In						0.6			
	In	3*a*	0	0	0.93	Tet	1.0	9.8	9.1	11.1
V	Zn	3*a*	0	0	0.40	Tet	0.3			
	Mn						0.2			
	In						0.5			
	Zn	3*a*	0	0	0.17	Oct	0.3			
	Mn						0.2			
	In						0.5			
	In	3*a*	0	0	0.93	Tet	1.0	10.9	9.9	13.6
VI	Zn	3*a*	0	0	0.40	Tet	0.6			
	Mn						0.2			
	In						0.2			
	In	3*a*	0	0	0.17	Oct	1.0			
	Mn	3*a*	0	0	0.93	Tet	0.2			
	In						0.8	14.9	12.4	25.3
VII	Zn	3*a*	0	0	0.40	Tet	0.4			
	Mn						0.2			
	In						0.4			
	In	3*a*	0	0	0.17	Oct	0.6			
	Zn	3*a*	0	0	0.93	Tet	0.2			
	Mn						0.2			
	In						1.0	14.0	12.0	22.3

the space group $R\bar{3}m$ in terms of a close packing of S atoms, with Zn atoms and half of the In atoms distributed at random in tetrahedral sites, while the other half of the In atoms were placed in octahedral sites. This distribution of ions produces a disordered layered structure. For the $Zn_{0.6}Mn_{0.4}In_2S_4$ alloy, the Mn atoms substitute Zn atoms in the structure of $ZnIn_2S_4$, preserving the centrosymmetry of the parent structure. As Table 2 shows, the fit of this model to the experimental diffraction data was poor, giving high figures of merit R_{wp} = 28.5% and R_p = 25.3%, for 26 variables. In particular, the reflection 006 has zero calculated intensity and therefore does not fit at all.

Table 2
Final atomic positions and isotropic temperature factors for the quaternary alloy $Zn_{0.6}Mn_{0.4}In_2S_4$, space group $R3m$, Z = 3, a = 3875 (2), c = 37208 (4) Å.

Atom	Occupancy	x	y	z	U_{iso} (Å^2)
Mn(1)	0.2				0.01311
Zn(1)	0.4	0	0	0.392584	0.01311
In(1)	0.4				0.01311
Mn(2)	0.2				0.01311
Zn(2)	0.2	0	0	0.161237	0.01311
In(2)	0.6				0.01311
In(3)	1.0	0	0	0.929657	0.01311
S(1)	1.0	0	0	0.036750	0.01119
S(2)	1.0	0	0	0.288360	0.01119
S(3)	1.0	0	0	0.458145	0.01119
S(4)	1.0	0	0	0.863597	0.01119

3.1.2. Non-centrosymmetric models in the *R*3*m* space group. In the model of Lappe *et al.* (1962), all the atoms occupy Wyckoff positions 3*a*, with the Zn atoms and half of the In atoms placed in separate tetrahedral positions. In this case, different distributions of cations in the tetrahedral and octahedral sites are feasible, which are summarized in Table 1. The cationic distribution in the different models is such that the local 3*m* symmetry is preserved. The best fit to the experimental data corresponded to model IV, in which the Mn ions occupy tetrahedral and octahedral positions adjacent in the cell, shared with the Zn and In atoms in Zn:Mn:In ratios of 0.4:0.2:0.4 and 0.2:0.2:0.6, respectively. The final Rietveld plot is shown in Fig. 1. There is significant improvement in the fit to the experimental profile, and in particular with the 006 reflection. Table 2 shows the final atomic positions and isotropic temperature factors for the $Zn_{0.6}Mn_{0.4}In_2S_4$ alloy.

3.2. Selected-area electron diffraction (SAED)

The reciprocal lattice along the [001] direction for the alloy $Zn_{0.6}Mn_{0.4}In_2S_4$ was studied using SAED patterns. Fig. 2 shows the pattern recorded on an image plate. The structural analysis, following standard electron diffraction procedures, reveals a rhombohedral unit with a = 3.06 Å.

3.3. High-resolution electron microscopy (HRTEM)

A digitalized high-resolution image of the alloy $Zn_{0.6}Mn_{0.4}In_2S_4$ along the [001] direction is shown in Fig. 3. Contrast changes due to thickness variations along vertical and horizontal directions are observed. The zone selected at the right of the image was processed with the program *CRISP* (Hovmöller, 1992) to obtain crystallographic phases imposing the *p*6 symmetry on the projection. The cell parameter a was found, giving a value of 21.5 Å, a multiple of 3.06 Å, with good discrepancy values of $R_{symmetry}$ = 15.3% and $\varphi_{residual}$ = 0.1.

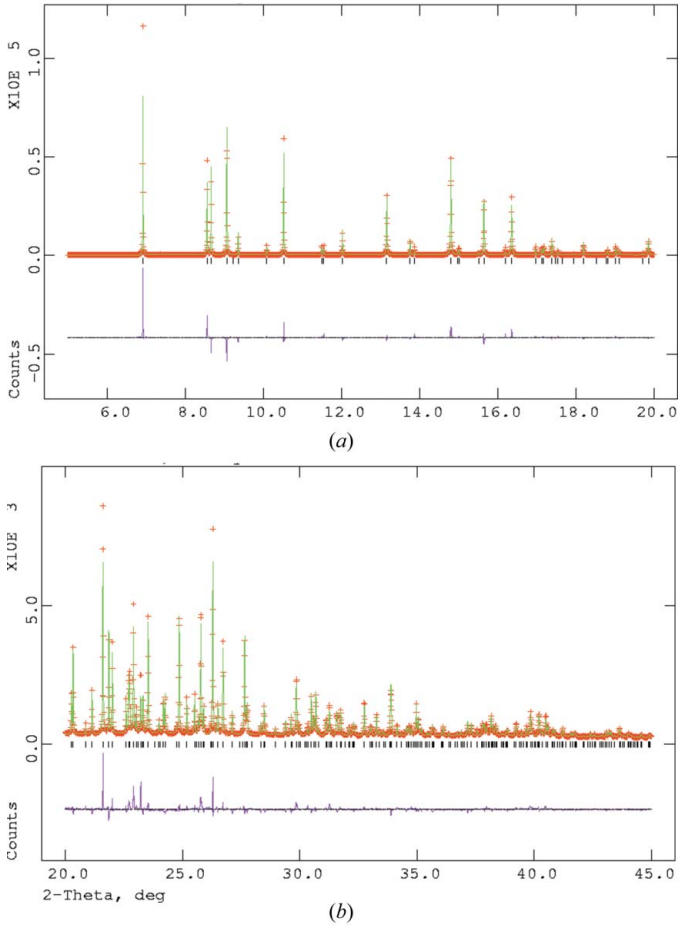

Figure 1
Final observed (points), calculated (lines), and difference profiles for the Rietveld refinement of the quaternary alloy $Zn_{0.6}Mn_{0.4}In_2S_4$ from high-resolution powder diffraction data. (*a*) Data from 5 to 20° 2θ. (*b*) Data from 20 to 45° 2θ.

3.4. Convergent-beam electron diffraction (CBED)

In the CBED patterns, the contrast details arising from the dynamical diffraction effects and the geometrical configurations derived from structural arrays in our samples, in direct and diffracted beams, allow the detection, identification and differentiation of space groups $R\bar{3}m$ and $R3m$ by checking the symmetry of the diffraction pattern obtained perpendicular to the [001] direction, as shown in Table 3 (Buxton *et al.*, 1976). Fig. 4 shows a micrograph for the alloy $Zn_{0.6}Mn_{0.4}In_2S_4$ collected at an acceleration potential of 150 kV, using a large convergence angle along [001], with its simulated image placed at its right. The pattern contains both zero-order Laue zone (ZOLZ) and high-order Laue zone (HOLZ) information, and Kikuchi lines. At the zero level, the pattern shows rotational symmetry of order 3, as shown by the triangle in the centre of the micrograph. Three mirror planes intercepting at angles of 120° are also depicted. In Table 3, the symmetries of the micrographs with rhombohedral cells perpendicular to [001] are given. All this information clearly points towards a micrograph with point symmetry 3*m*. Therefore, it can be concluded unambiguously that the structure of the quaternary alloy is non-centrosymmetric *R*3*m*.

Table 3
Zone-axis symmetry for the [001] direction for the point groups $\bar{3}m$ and 3*m* from Buxton *et al.* (1976).

Point group	[001]
$\bar{3}m$	$6mm_R$
3*m*	3*m*

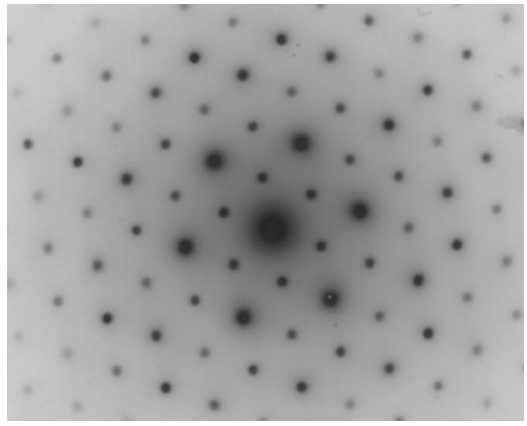

Figure 2
SAED of $Zn_{0.6}Mn_{0.4}In_2S_4$ along the [001] direction.

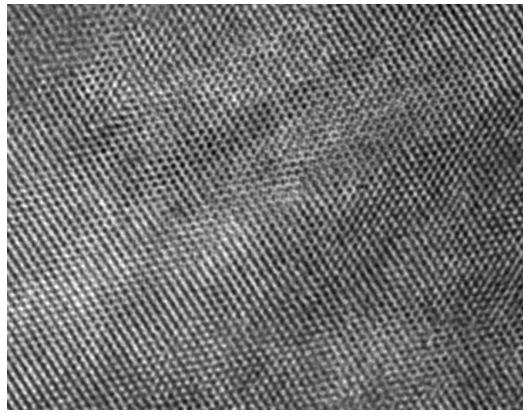

Figure 3
HRTEM of the alloy $Zn_{0.6}Mn_{0.4}In_2S_4$.

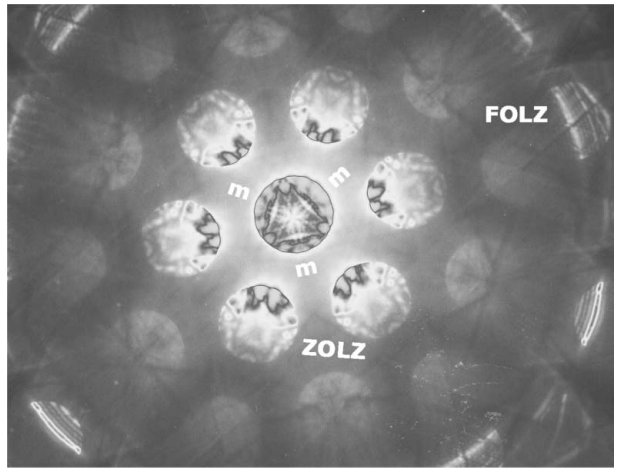

Figure 4
CBED patterns of the alloy $Zn_{0.6}Mn_{0.4}In_2S_4$ at 150 kV.

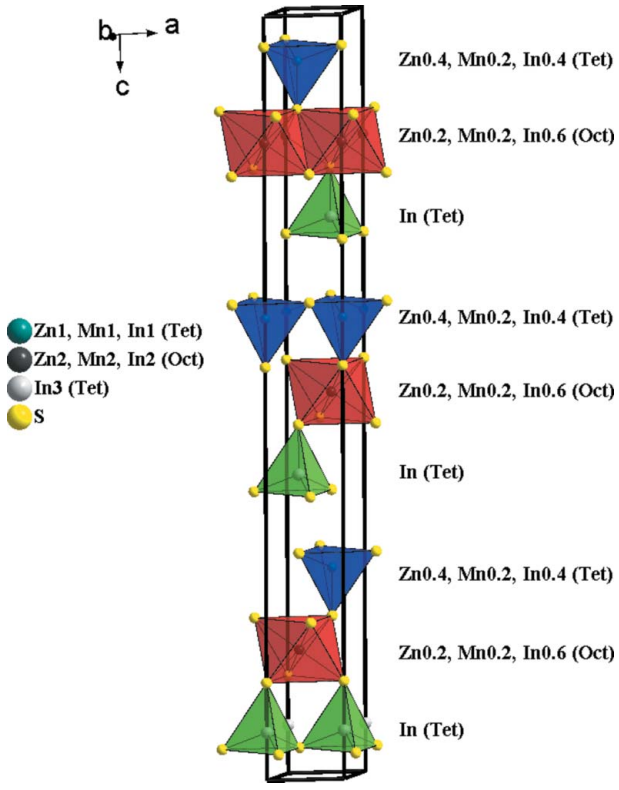

Figure 5
A view showing the unit cell of the $Zn_{0.6}Mn_{0.4}In_2S_4$ structure (model IV) in the *R*3*m* space group.

4. Conclusions

The quaternary alloy $Zn_{0.6}Mn_{0.4}In_2S_4$ shows a rhombohedral layered crystal structure, in space group *R*3*m* (160). The sequence of layers is:

$$SIn_{tet}S(Zn_{0.2}Mn_{0.2}In_{0.6})_{oct}S(Zn_{0.4}Mn_{0.2}In_{0.4})_{tet}S\ldots SIn_{tet}.$$

A diagram of the layers in the structure along the *c* axis is shown in Fig. 5. The 3*m* symmetry of a CBED micrograph with zone-axis [001] confirmed the space-group symmetry *R*3*m*. The Zn, Mn and In atoms occupy both tetrahedral and octahedral sites in the structure in a disordered way, but in such proportions that the local $\bar{3}m$ symmetry of the parent compound, $ZnIn_2S_4$, is broken.

We thank the ESRF for providing synchrotron radiation beam time, FONACIT-Venezuela and CDCHT-ULA.

References

Atwood, J. L., Davies, J. E. & MacNicold, D. D. (1984). *Inclusion Compounds*, Vols. I, II, III. New York: Academic Press.
Berand, N. & Range, K. J. (1994). *J. Alloys Compd.* **205**, 295–301.
Boultif, A. & Louër, D. (1991). *J. Appl. Cryst.* **24**, 987–993.
Buxton, B. F., Eades, J. A., Steeds, J. W. & Rackham, G. M. (1976). *Philos. Trans. R. Soc. London Ser. A*, **281**, 171–194.
Dollase, W. A. (1986). *J. Appl. Cryst.* **19**, 267–272.
Finger, L. W., Cox, D. E. & Jephcoat, A. P. (1994). *J. Appl. Cryst.* **27**, 892–900.
Fitch, A. N. (1996). *Mater. Sci. Forum*, **228–231**, 219–222.
Fitch, A. N. (2004). *J. Res. Natl Inst. Stand. Technol.* **109**, 133–142.
Fontal, B., López-Rivera, S. A., Martínez, L. & Giriat, W. (1996). *Semicond. Sci. Technol.* **11**, 1056–1058.
Giriat, W. (1985). *Phys. Status Solidi B*, **132**, K131–K132.
Hovmöller, S. (1992). *Ultramicroscopy*, **41**, 121–135.
Laar, B. van & Yelon, W. B. (1984). *J. Appl. Cryst.* **17**, 47–54.
Lappe, F., Niggli, A., Nitsche, R. & White, J. G. (1962). *Z. Kristallogr.* **117**, 146–152.
Larson, A. C. & Von Dreele, R. B. (2001). *General Structure Analysis System* (*GSAS*). Report LAUR 86-748, Los Alamos National Laboratory, USA.
López-Rivera, S. A., Mora, A. J., Acosta-Najarro, D., Rivera, A. V. & Ávila-Godoy, R. (2001). *Semicond. Sci. Technol.* **16**, 367–371.
Lutz, H. D. & Jun, M. (1989). *Z. Anorg. Allg. Chem.* **579**, 57–67.
Pineda, C., Martín, J. M. & López-Rivera, S. A. (1998). *Rev. Mex. Fís.* **44**, 224–227.
Rietveld, H. M. (1967). *Acta Cryst.* **22**, 151–152.
Sagredo, V., Betancourt, L., Chourio, M., Attolini, G. & Pelosi, C. (1993). *Jpn J. Appl. Phys.* **32**, 391–392.
Smith, G. S. & Snyder, R. L. (1979). *J. Appl. Cryst.* **12**, 60–65.
Sombuthawee, C., Bonsall, S. B. & Hummel, F. A. (1978). *J. Solid State Chem.* **25**, 391–399.
Tatsi, A., Lampakis, D., Liarokapis, E., López-Rivera, S. A. & Martínez, L. (2002). *High Pressure Res.* **22**, 89–93.
Wakaki, M., Ogawa, T. & Arai, T. (1983). *Nuovo Cimento D*, **2**, 1809–1813.
Wolff, P. M. de (1968). *J. Appl. Cryst.* **1**, 108–113.